AIAA 2013-1933

SDM 2013 Student Papers Competition

Continuum Shape Sensitivity with Spatial Gradient Reconstruction of Built-up Structures*

David M. Cross† and Robert A. Canfield‡
Virginia Tech, Blacksburg, VA, 24061, USA

Accurate and efficient computation of sensitivities are critical to the success of implementing gradient based optimization algorithms for large-scale, multi-disciplinary design problems. Traditional methods for computing design sensitivities, such as the finite difference, complex step, discrete semi-analytic, and discrete analytic methods often yield unsatisfactory results. Presented here is a local continuum shape sensitivity method with spatial gradient reconstruction. This method is accurate, efficient, and easy to implement. Most importantly, it is formulated as a general approach to sensitivity analysis, which makes it amenable to use with black box analyses. The method has previously been implemented for beam models, and here it is implemented for linear static bending of rectangular stiffened plate models. Among the examples presented are rectangular plates analysed with a variety of pressure loads, boundary conditions, plate theories, and finite element formulations. The final implementation is for a beam-stiffened rectangular plate, which is representative of a built-up structure. The local continuum sensitivity solutions are compared to either analytically derived sensitivities or finite difference sensitivities.

Nomenclature

$\boldsymbol{A}$	General time-space differential operator
$\boldsymbol{b}$	Design variable (shape parameter)
$\boldsymbol{B}$	General boundary operator
δ	Perturbation
∇	Gradient operator
Δ	Essential boundary displacement
$\boldsymbol{f}$	Generalized loads (body forces)
Γ	Spatial boundary
$\boldsymbol{g}$	Boundary loads
M	Internal bending moment
Ω	Spatial domain
ψ	Rotation
$\boldsymbol{u}$	Primary response variable (displacement)
$\mathcal{V}$	Design velocity
V	Internal shear force
w	Transverse displacement
$\boldsymbol{x}$	Vector of spatial coordinates

** The views and conclusions contained herein are those of the authors and should not be interpreted as necessarily representing the official policies or endorsements, either expressed or implied, of Air Force Research Laboratory or the U.S. Government.*

†Ph.D. Candidate, Department of Aerospace and Ocean Engineering, Virginia Tech, 215 Randolph Hall, Blacksburg, VA, 24061, AIAA Member.

‡Professor, Department of Aerospace and Ocean Engineering, Virginia Tech, 214 Randolph Hall, Blacksburg, VA, 24061, AIAA Associate Fellow.

I. Introduction

The mission profiles of unmanned aerial vehicles are pushing the bounds of the design envelope towards novel aircraft configurations that exist well outside the scope of traditional aircraft design methods. Multidisciplinary design optimization (MDO) can be used to explore the vast and complicated design spaces in which these novel configurations exist. Gradient-based optimization algorithms are often used in MDO frameworks. Therefore, design sensitivities are required for every analysis routine included in the MDO framework. For large-scale design problems involving high-fidelity, nonlinear analysis numerical sensitivity methods often are computationally expensive and have limited accuracy. For this reason, much attention has been given to analytic sensitivity methods.[1]

The derivation of analytic sensitivities is typically quite rigorous and in most cases requires access to the analysis formulation and/or source code. This requirement limits the use of black box analysis tools. Commercial codes, such as Nastran, may see limited use in these computational MDO environments because they do not calculate accurate sensitivities for high-fidelity analysis. One reason research codes are being heavily used in the development of computational MDO environments is because sensitivity packages can be developed as part of the reasearch code.

In this paper a local continuum sensitivity method with spatial gradient reconstruction is presented. The unique way in which this analytic sensitivity method is implemented eliminates the required access to the source code. In effect the analysis tool can be treated as a black box, while still achieving analytic sensitivities. After reviewing the current literature on continuum sensitivity analysis (CSA); the development of said method is described.

CSA involves solving a set of partial differential equations called the continuum sensitivity equations (CSEs). CSA has several computational efficiencies that other sensitivity formulations do not have.[2] Aurora and Haug[3] followed by Dems, Mroz, and Haftka[4,5] were among the first to introduce CSA for structural problems. Bhaskaran and Berkooz presented a CSA solution for a two-dimensional elastic structure.[6] Furthermore, Choi and Kim documented CSA formulation for structural optimization extensively.[7] Borgaard and Burns applied CSA in a fluid setting with a formulation for aerodynamic design.[8,9] They followed up this work with other applications of CSA to fluid flow optimization, as did Stanley and Stewart.[10] Pelletier, Turgeon, Borggaard, and Etienne have applied CSA to numerous fluid-structure interaction (FSI) problems, but focused on sensitivities of fluid flow parameters for nearby problems.[11,12] Most recently, Wickert, Liu, Cross, and Canfield have employed CSA for shape optimization of nonlinear structures subject to an aeroelastic gust response.[1,13–19]

All implementations of CSA previously mentioned have one thing in common; they all require access to the analysis formulation and/or source code. Haftka specifically discusses that the discrete analytic sensitivity method is not "easily amenable" to general-purpose structural analysis tools.[20] Furthermore, he states that the semi-analytic method is an insufficient and unreliable substitute for certain shape sensitivity problems.[21] Duvigneau and Pelletier detail a method for reconstructing high order spatial derivatives as a necessary step to accurately solving their fluid sensitivity solutions.[22] Implementing a variation of their method in combination with the unique sensitivity formulation presented here yields an approach that accurately computes analytic shape sensitivities with black box analysis tools.

After the local continuum sensitivity method with spatial gradient reconstruction (SGR) is formulated, it is implemented on a series of structural shape sensitivity problems. The first is the shape sensitivity of a linear static bending response of a simply-supported rectangular plate to different loading conditions, with different shape parameterizations, and modeled with different finite element formulations. The second implementation is on a thick rectangular plate with mixed boundary conditions, modeled using both Kirchoff and Reissner-Midlin plate theories. Lastly, the sensitivity method is implemented for a beam-stiffened rectangular plate, which is representative of a built-up structure. The various implementations help demonstrate the specific advantages of the sensitivity approach. Choi and Kim[7] compute shape sentivity for several plate problems, but always use the total continuum sensitivity method and always assume some knowledge of the analysis formulation.

II. Comparison of Sensitivity Formulations

Figure 1 is a taxonomy of sensitivity formulations. The numeric methods suffer from being computationally expensive and inaccurate. The analytic methods overcome the pitfalls of the numeric methods, but typically involve a rigorous formulation and implementation. A closer look at each of the analytic sensitivity methods promotes an understanding of the local continuum sensitivity method presented here.

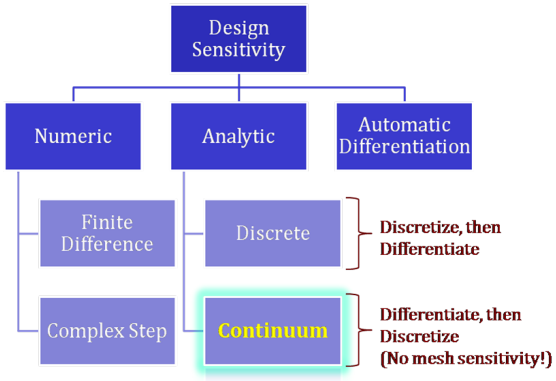

Figure 1. Taxonomy of Sensitivity Formulations

A. Analytic Sensitivity Methods

Analytic sensitivity methods can be more accurate and computationally efficient than the numeric methods. This depends on the formulation of the pseudo loads that appear in the sensitivity equations. Let the boundary value system in Eqs. (1) and (2) represent the simulation scheme.

$$\boldsymbol{A}(\boldsymbol{u};\boldsymbol{b}) = \boldsymbol{f}(\boldsymbol{x};\boldsymbol{b}) \quad on \quad \Omega \tag{1}$$

$$\boldsymbol{B}(\boldsymbol{u};\boldsymbol{b}) = \boldsymbol{g}(\boldsymbol{x};\boldsymbol{b}) \quad on \quad \Gamma \tag{2}$$

Where, $\boldsymbol{A}$ and $\boldsymbol{B}$ are the time-space differential operator and the boundary condition operator, respectively, which specify the governing equations. In addition, $\boldsymbol{u}$ is a vector of response variables, $\boldsymbol{b}$ is a vector of design variables, and $\boldsymbol{x}$ is a vector of spatial coordinates. For the purposes of this paper an analytic sensitivity method is classified as either a discrete or continuum method. Discrete sensitivity equations are obtained by discretizing Eqs. (1) and (2) and then differentiating the resulting discrete system. In contrast, the continuum sensitivity equations are obtained by first differentiating Eqs. (1) and (2) with respect to shape design variables and then discretizing the resulting continuous system.[1]

Either total or local differentiation can be used. Typically, for shape optimization of structures, the material derivative or total sensitivity is required. Therefore, total differentiation is most commonly used for discrete analytic and total continuum sensitivity analysis of structural applications. However, it is possible to use local differentiation and transform the local sensitivity solution into a total sensitivity. This transformation is defined by the material or total derivative definition in Eq. (3).

$$\frac{D\boldsymbol{u}}{Db_i} = \frac{\partial \boldsymbol{u}}{\partial b_i} + \frac{\partial \boldsymbol{u}}{\partial \boldsymbol{x}} \cdot \frac{\partial \boldsymbol{x}}{\partial b_i} \tag{3}$$

The left hand side denotes the material derivative of response variables, $\boldsymbol{u}$ with respect to the i-th design variable, b_i. The material derivative consists of the local design derivative, $\frac{\partial \boldsymbol{u}}{\partial b}$, plus a convective term, $\frac{\partial \boldsymbol{u}}{\partial \boldsymbol{x}} \cdot \frac{\partial \boldsymbol{x}}{\partial b}$. The local design derivative is a measure of the rate of change of the response at a fixed point in the global reference frame due to the rate of change of a design parameter. The convective term accounts for the movement of a material point should the geometric domain, $\boldsymbol{x}$ change with the design parameter. For value parameters the local design sensitivity is equivalent to the total design sensitivity, and for shape parameters

the nonzero convective term is the difference between the local and total design sensitivities. Eq. (3) can be written in compact notation as

$$\dot{\boldsymbol{u}} = \boldsymbol{u}' + \nabla \boldsymbol{u} \cdot \boldsymbol{\mathcal{V}} \tag{4}$$

Using the total derivative definition in Eq. (4) to differentiate Eq. (1) yields the total continuum sensitivity system in Eq. (5).

$$\bar{\boldsymbol{A}}_{Total}(\dot{\boldsymbol{u}}; \boldsymbol{b}) = \dot{\boldsymbol{f}}(\boldsymbol{x}; \boldsymbol{b}) - \dot{\boldsymbol{A}}(\boldsymbol{u}; \boldsymbol{b}) \quad on \quad \Omega \tag{5}$$

In contrast, discretizing Eq. (1) yields the discrete system in Eq. (6), upon which total differentiation yields the discrete sensitivity system in Eq. (7). Akbari and Kim have shown that under certain conditions once Eq. (5) is discretized it is equivalent to Eq. (7).[23] This means, that for most structural problems, the total continuum and discrete sensitivity methods are equivalent.

$$[K]\{u\} = \{f\} \tag{6}$$

$$[K]\{\dot{u}\} = \{\dot{f}\} - [\dot{K}]\{u\} \tag{7}$$

The first term on the right hand side of Eq. (7) is referred to as the external fictitious load and is easily derived from the applied external load and the design geometry. The second term on the right hand side of Eq. (7) is referred to as the structural fictitious load. This term contains the derivative of the stiffness matrix.[7] Analytic formulation of this term requires access to the source code, which makes the total continuum and discrete methods infeasible to implement with black box tools. This is why the discrete semi-analytic method is commonly used. However, numerical error that arises from finite differencing the stiffness matrix can result in poor sensitivities, especially for shape parameters.

Local differentiation of Eqs. (1) and total differentiation of (2), after rearranging terms, yields the local continuum sensitivity system.

$$\bar{\boldsymbol{A}}_{Local}(\boldsymbol{u}'; \boldsymbol{b}) = \boldsymbol{f}'(\boldsymbol{x}; \boldsymbol{b}) - \boldsymbol{A}'(\boldsymbol{u}; \boldsymbol{b}) \quad on \quad \Omega \tag{8}$$

$$\bar{\boldsymbol{B}}_{Local}(\boldsymbol{u}'; \boldsymbol{b}) = \dot{\boldsymbol{g}}(\boldsymbol{x}; \boldsymbol{b}) - \nabla \boldsymbol{B}(\boldsymbol{u}; \boldsymbol{b}) \cdot \mathcal{V} \quad on \quad \Gamma \tag{9}$$

Typically, for structural elasticity problems and fluid flow problems, the structural fictitious load, $\boldsymbol{A}'$ is zero. However, the boundary conditions of the sensitivity equations contain a structural fictitious load in the form of $\nabla \boldsymbol{B}(\boldsymbol{u}; \boldsymbol{b})$. Analytic formulation of this term requires knowledge of the boundary operator formulation. The following sections detail how to numerically approximate this term in order to sufficiently achieve an accurate solution to the analytic local continuum sensitivity equations.

III. Local Continuum Sensitivity with Spatial Gradient Reconstruction

If the $\nabla \boldsymbol{B}(\boldsymbol{u}; \boldsymbol{b})$ term in Eq. (9) can be sufficiently approximated directly from analysis results, then the local continuum sensitivity method can be implemented for black box analyses. A specific approach to accomplish said approximation is presented here.

A. Numerical Approximation of Local Continuum Boundary Conditions

In order to solve the local sensitivity system numerically, Eqs. (8) and (9) must be discretized and the sensitivity boundary conditions must be derived. When Eq. (1) is linear, than $\bar{\boldsymbol{A}}_{Local} = \boldsymbol{A}$. Therefore, the coefficient matrix of the local sensitivity system is simply the linear stiffness matrix of the finite element analysis. If the analysis tool being used can output the stiffness matrix, then it can be used to discretize the left hand side of Eq. (8). As previously mentioned, all of the right hand side terms are easily derived except for $\nabla \boldsymbol{B}(\boldsymbol{u}; \boldsymbol{b})$.

Approximation of the gradient of the boundary operator, $\nabla \boldsymbol{B}(\boldsymbol{u}; \boldsymbol{b})$ requires taking a closer look at the specific boundary conditions of the original analysis system. Each boundary condition will either be an essential boundary condition or a natural boundary condition. An essential boundary condition is a special case of Eq.(2).

$$\boldsymbol{u}|_{\Gamma} = \boldsymbol{g}(\boldsymbol{x}; \boldsymbol{b}) \tag{10}$$

Taking the material derivative of Eq. (10) and rearranging terms according to Eq. (9), the essential sensitivity boundary condition becomes

$$\boldsymbol{u}'|_{\Gamma} = \dot{\boldsymbol{g}}(\boldsymbol{x};\boldsymbol{b}) - \nabla\boldsymbol{u}|_{\Gamma} \cdot \boldsymbol{\mathcal{V}} \tag{11}$$

A similar formulation is used for a natural boundary condition.

$$L(\boldsymbol{u};\boldsymbol{b})|_{\Gamma} = \boldsymbol{g}(\boldsymbol{x};\boldsymbol{b}) \tag{12}$$

$$L(\boldsymbol{u}';\boldsymbol{b})|_{\Gamma} = \dot{\boldsymbol{g}}(\boldsymbol{x};\boldsymbol{b}) - \nabla L(\boldsymbol{u};\boldsymbol{b})|_{\Gamma} \cdot \boldsymbol{\mathcal{V}} \tag{13}$$

For an essential boundary condition $\nabla\boldsymbol{B}(\boldsymbol{u};\boldsymbol{b}) = \nabla\boldsymbol{u}$, and for a natural boundary condition $\nabla\boldsymbol{B}(\boldsymbol{u};\boldsymbol{b}) = \nabla L(\boldsymbol{u};\boldsymbol{b})$. For a displacement based finite element structural analysis, $\boldsymbol{u}$ is a displacement and $L(\boldsymbol{u};\boldsymbol{b})$ is an internal force, such as moment or shear. Both displacements and internal forces are typical outputs of finite element solvers. Therefore, it is reasonable to expect that the spatial gradients of $\boldsymbol{u}$ and $L(\boldsymbol{u};\boldsymbol{b})$ can be numerically approximated from the analysis output.

In summary, the conditions under which the local continuum sensitivity of a black box analysis can be solved are

1. The black box solver must output the system matrices.
2. The black box solver must output analysis response data $\boldsymbol{u}$ (displacements, velocities, accelerations, temperature, etc.).
3. The black box solver must output the element force data $L(\boldsymbol{u};\boldsymbol{b})$ (axial and shear forces, internal bending moments, pressure forces, etc.).
4. The user must be able to accurately reconstruct $\nabla\boldsymbol{u}|_{\Gamma}$ and $\nabla L(\boldsymbol{u};\boldsymbol{b})|_{\Gamma}$ from $\boldsymbol{u}$ and $L(\boldsymbol{u};\boldsymbol{b})$ in order to formulate the sensitivity boundary conditions.
5. The user must be able to accurately reconstruct $\nabla\boldsymbol{u}|_{\Omega}$ from $\boldsymbol{u}$ in order to convert the local sensitivities into total sensitivities as a final post-processing step.

B. Taylor Series l-patch Method

Zienkiewicz and Zhu present a patch technique to recover spatial derivatives of response data.[24] Duvigneau and Pelletier,[22] following the work of Zienkewicz and Zhu, present a similar method, which they use to recover spatial derivatives of response data specifically on the boundary. Their method can be adapted to satisfy the fourth condition listed above. A 2-D formulation of the method begins with a Taylor series expansion of an arbitrary response variable, φ about a boundary node P.

$$\varphi(x,y) = \varphi(x_P,y_P)+(x-x_P)\varphi_x+(y-y_P)\varphi_y+\frac{1}{2}(x-x_P)^2\varphi_{xx}+(x-x_P)(y-y_P)\varphi_{xy}+\frac{1}{2}(y-y_P)^2\varphi_{yy}+... \tag{14}$$

The response variable, φ and its derivatives can be determined through a least squares match of the Taylor series to the analysis response at a set of nodes, $N(x_n,y_n)$ within a patch $\mathcal{P}$ surrounding node P. That is, solve

$$\min \mathcal{J}(\mathbf{y}_{\varphi}) = \frac{1}{2}\sum_{N\in\mathcal{P}}(\mathbf{B}^T\mathbf{y}_{\varphi} - \varphi_N)^2 \tag{15}$$

Where,

$$\varphi_N = \varphi(x_n,y_n) \tag{16}$$

$$\mathbf{B}^T = \{\ 1 \quad x_n - x_P \quad y_n - y_P \quad \tfrac{1}{2}(x_n-x_P)^2 \quad (x_n-x_P)(y_n-y_P) \quad \tfrac{1}{2}(y_n-y_P)^2 \quad ...\ \} \tag{17}$$

$$\mathbf{y}_{\varphi}^T = \{\ \varphi \quad \varphi_x \quad \varphi_y \quad \varphi_{xx} \quad \varphi_{xy} \quad \varphi_{yy} \quad ...\ \} \tag{18}$$

The coordinate dimensions of the Taylor series should be adjusted as necessary to match the dimensions of the problem. The l in Taylor series l-patch method stands for"layer". Duvigneau and Pelletier define the element patch, $\mathcal{P}$ by layers. A 1-layer patch includes only the elements which contain the boundary node P. A 2-layer patch also includes elements which are adjacent to the elements of a 1-layer patch. A 3-layer patch also includes elements adjacent to elements of a 2-layer patch, and so forth. Figure 2 illustrates

various patch definitions. The accuracy of the spatial derivative reconstruction depends on three things. First, it depends on the accuracy of the response itself, and second, it depends on the order of the Taylor series expansion. Lastly, it depends on the number of layers in the patch. More details on these issues can be found in Ref. (22).

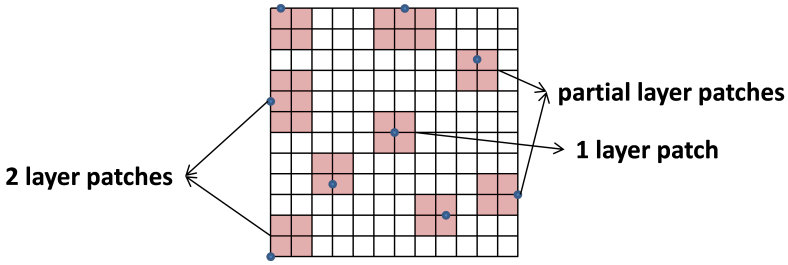

Figure 2. Examples of Patch Definitions

Spatial gradient reconstruction (SGR) is used throughout this paper to approximate spatial derivatives of dispalcements and forces of rectangula rplate models. When implmenting SGR for these 2-D problems, the patches were not directly defined by a number of layers, but rather an x- and y- distance, Δx and Δy, respectively. Nodes that were within $\pm\Delta x$ in the x-direction and $\pm\Delta y$ in the y-direction of node P were included in the patch. Uniform meshes are used for all of the problems, and the element size is defined by δx and δy. The distances, Δx and Δy were consistently chosen to be equal to $4\delta x$ and $4\delta y$, respectively. When SGR was being used for displacements a fourth order Taylor series was used, and when SGR was being used for forces a third order Taylor series was used. The accuracy of this specific SGR computation is addressed in the next section.

IV. Continuum Sensitivity Implementation for Linear Static Bending of Rectangular Plate Models

The following sections show various implementations of the local continuum sensitivity method with spatial gradient reconstruction (SGR). The examples are designed to highlight the versatility and generality of this sensitivity approach, as well as indicate areas where the current implementation needs to be improved.

A. Standard Formulation of Local Sensitivity Boundary Conditions

Assume the plate is in the x-y plane and has three degrees of freedom, transverse displacement, w, rotation about the x-axis, ψ_x, and rotation about the y-axis, ψ_y. Furthermore, the plate's edges can either be clamped, simply-supported, or free. Since the plate is 2-D, $\boldsymbol{\mathcal{V}}$ from Eq. (9) is a vector containing design velocity functions in both the x- and y- directions and takes the definition shown in Eq. (19). Design velocity functions parameterize how the domain changes with the design variables. From Eq. (9), ∇ is defined in 2-D by Eq. (20).

$$\boldsymbol{\mathcal{V}} = \mathcal{V}_x\hat{x} + \mathcal{V}_y\hat{y} \tag{19}$$

$$\nabla = \frac{\partial}{\partial x}\hat{x} + \frac{\partial}{\partial y}\hat{y} \tag{20}$$

Figure (3) shows the forces that act on the plate element. Only out-of-plane loads are applied for the examples presented here, and linear theory does not include membrane-bending coupling; therefore, the in-plane loads can be neglected. This information, along with Eq. (9), is used to formulate the local sensitivity boundary conditions for a rectangular plate in the x-y plane. For the first degree of freedom on the boundary Γ_v, either

$$w' = \dot{w} - w_{,x}\cdot\mathcal{V}_x - w_{,y}\cdot\mathcal{V}_y \quad \text{or} \quad V_s' = \dot{V}_s - V_{s,x}\cdot\mathcal{V}_x - V_{s,y}\cdot\mathcal{V}_y \tag{21}$$

For the second degree of freedom on the boundary Γ_v, either

$$\psi_x' = \dot{\psi}_x - \psi_{x,x}\cdot\mathcal{V}_x - \psi_{x,y}\cdot\mathcal{V}_y \quad \text{or} \quad M_s' = \dot{M}_s - M_{s,x}\cdot\mathcal{V}_x - M_{s,y}\cdot\mathcal{V}_y \tag{22}$$

For the third degree of freedom on the boundary Γ_v, either

$$\psi'_y = \dot{\psi}_y - \psi_{y,x} \cdot \mathcal{V}_x - \psi_{y,y} \cdot \mathcal{V}_y \quad \text{or} \quad M'_v = \dot{M}_v - M_{v,x} \cdot \mathcal{V}_x - M_{v,y} \cdot \mathcal{V}_y \tag{23}$$

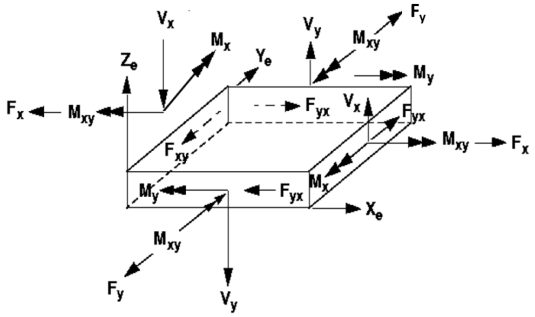

Figure 3. Forces Acting on a Plate Element

B. Distributed Transverse Loading of Simply-Supported Rectangular Plates

The following is a comparison of analytic and finite element plate bending solutions for a simply-supported rectangular plate under a distributed sinusoidal transverse load. The analytic solution comes from *Theory of Plates and Shells* by Timoshenko and utilizes Kirchhoff plate theory.[25] Shape sensitivities are calculated from the finite element response by implementing the local continuum sensitivity method with SGR. These computational sensitivities are compared to analytic sensitivity solutions derived from the analytic plate response.

1. *Model Information*

The governing equation of the analytic plate bending solution is a special case of Eq. (1)

$$A(w;\boldsymbol{b}) = \frac{\partial^4 w}{\partial x^4} + 2\frac{\partial^2 w}{\partial x^2}\frac{\partial^2 w}{\partial y^2} + \frac{\partial^4 w}{\partial y^4} = f(x,y;\boldsymbol{b}) \tag{24}$$

Where $w(x,y)$ is the transverse displacement and $f(x,y;\boldsymbol{b})$ is the distributed load.

$$f(x,y;\boldsymbol{b}) = \frac{q_0}{D}\sin\frac{\pi x}{a}\sin\frac{\pi y}{b} \tag{25}$$

In the above, a and b are the length dimensions of the plate in the x- and y- directions, respectively, q_0 is the load intensity at the center of the plate, and D is the flexural rigidity of an isotropic plate.

$$D = \frac{Et^3}{12\,(1-\nu^2)} \tag{26}$$

Since Kirchhoff plate thoery assumes small deflections and rotations, the plate rotations are related to the slopes by the expressions in Eq. (27).

$$\psi_x(w) = \frac{\partial w(x,y)}{\partial y} \quad , \quad \psi_y(w) = -\frac{\partial w(x,y)}{\partial x} \tag{27}$$

Furthermore, the moments are related to w by the expressions in Eq. (28).

$$M_x(w) = D\left(\frac{\partial^2 w(x,y)}{\partial x^2} + \nu\frac{\partial^2 w(x,y)}{\partial y^2}\right) \quad , \quad M_y(w) = D\left(\frac{\partial^2 w(x,y)}{\partial y^2} + \nu\frac{\partial^2 w(x,y)}{\partial x^2}\right) \tag{28}$$

The boundary conditions at $x = 0$ and $x = a$ are a special case of Eq. (2).

$$\boldsymbol{B}_{\Gamma_y}(w;\boldsymbol{b}) = \{w, \psi_x(w), M_x(w)\}^T = \{0,0,0\}^T = \boldsymbol{g}_{\Gamma_y}(x,y;\boldsymbol{b}) \tag{29}$$

The boundary conditions at $y = 0$ and $y = b$ are a special case of Eq. (2).

$$\boldsymbol{B}_{\Gamma_x}(w;\boldsymbol{b}) = \{w, M_y(w), \psi_y(w)\}^T = \{0,0,0\}^T = \boldsymbol{g}_{\Gamma_x}(x,y;\boldsymbol{b}) \tag{30}$$

The properties of the plate for the solution shown here are $a = 1m$, $b = 1.5m$, $q_0 = 100000N/m$, $E = 7e10N/m^2$, $t = 0.01m$, and $\nu = 0.25$. The finite element solution shown in the figures that follow is the result of a linear static analysis in Nastran with a 30 by 30 mesh of quadrilateral (CQUAD4) plate elements. In Figures (4) through (11), the surface represents the analytic solution, and the black dots represent the computational solution as approximated by or derived from the finite element analysis results. The only shape sensitivity solution presented here is the sensitivity of the plate response to a change in the plate dimension a. Therefore, it can be stated that $\boldsymbol{b} = a$.

2. *Displacements*

The analytic solutions of transverse displacement, rotation about the x-axis, and rotation about the y-axis are provided below. Figure (4) shows the finite element solution to be accurate.

$$w(x,y) = \frac{q_0}{D\pi^4}\frac{a^4b^4}{(a^2+b^2)^2}\sin\frac{\pi x}{a}\sin\frac{\pi y}{b} \tag{31}$$

$$\psi_x(x,y) = \frac{q_0}{D\pi^3}\frac{a^4b^3}{(a^2+b^2)^2}\sin\frac{\pi x}{a}\cos\frac{\pi y}{b} \tag{32}$$

$$\psi_y(x,y) = -\frac{q_0}{D\pi^3}\frac{a^3b^4}{(a^2+b^2)^2}\cos\frac{\pi x}{a}\sin\frac{\pi y}{b} \tag{33}$$

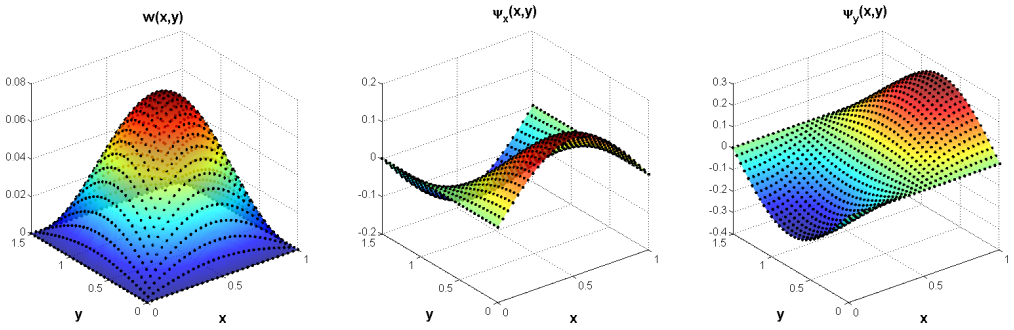

Figure 4. Displacements

3. *Displacement Gradients*

When the sensitivity variable a is perturbed, the plate geometry changes only in the x-direction. Therefore, the sensitivity analysis only requires spatial derivatives of response variables in the x-direction. The analytic solutions of the spatial derivatives in the x-direction of transverse displacement, rotation about the x-axis, and rotation about the y-axis given in Eqs. (34) through (36) are shown as color surface plots in Figure (5). Comparison with the SGR from the finite element response (black dots) demonstrates its accuracy.

$$w_{,x}(x,y) = \frac{q_0}{D\pi^3}\frac{a^3b^4}{(a^2+b^2)^2}\cos\frac{\pi x}{a}\sin\frac{\pi y}{b} \tag{34}$$

$$\psi_{x,x}(x,y) = \frac{q_0}{D\pi^2}\frac{a^3b^3}{(a^2+b^2)^2}\cos\frac{\pi x}{a}\cos\frac{\pi y}{b} \tag{35}$$

$$\psi_{y,x}(x,y) = \frac{q_0}{D\pi^2}\frac{a^2b^4}{(a^2+b^2)^2}\sin\frac{\pi x}{a}\sin\frac{\pi y}{b} \tag{36}$$

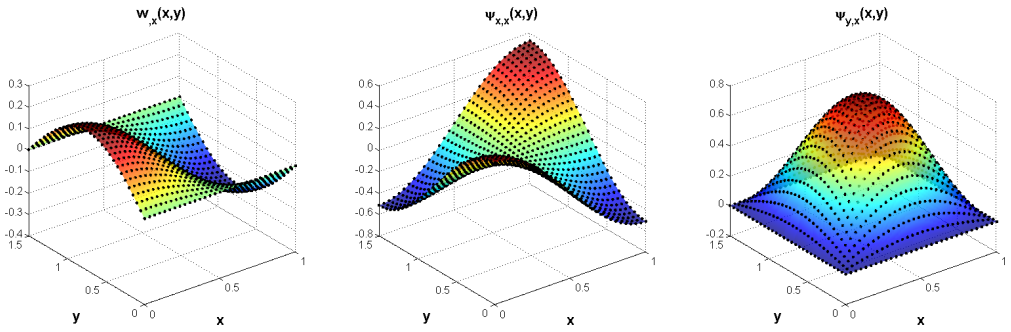

Figure 5. Displacement Gradients

4. Internal Forces and Internal Force Gradients

The moments about the x- and y- axes are the only internal forces that appear in the boundary conditions of the simply-supported plate. Therefore, the sensitivity analysis requires the spatial derivative of the moments in the x-direction. The analytic solutions of the moment about the y-axis and its spatial derivative in the x-direction are given in Eqs. (37) and (38) and shown as color surfaces in Figure (6). The black dots represent the finite element approximation of M_x and the SGR of $M_{x,x}$, respectively.

$$M_x(x,y) = D\left(\frac{\partial^2 w}{\partial x^2} + \nu\frac{\partial^2 w}{\partial y^2}\right) = \frac{q_0}{\pi^2}\frac{\left(a^2b^4 + \nu a^4b^2\right)}{\left(a^2+b^2\right)^2}\sin\frac{\pi x}{a}\sin\frac{\pi y}{b} \tag{37}$$

$$M_{x,x}(x,y) = D\frac{\partial}{\partial x}\left(\frac{\partial^2 w}{\partial x^2} + \nu\frac{\partial^2 w}{\partial y^2}\right) = \frac{q_0}{\pi}\frac{\left(ab^4 + \nu a^3b^2\right)}{\left(a^2+b^2\right)^2}\cos\frac{\pi x}{a}\sin\frac{\pi y}{b} \tag{38}$$

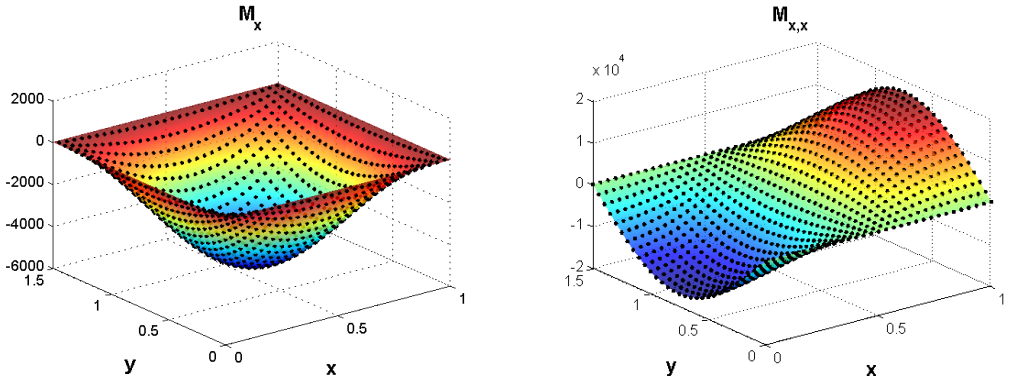

Figure 6. Moment about y-axis, M_x (left) and Spatial Derivative of Moment about y-axis, $M_{x,x}$ (right)

The analytic solution of the moment about the x-axis and its spatial derivative in the x-direction are given in Eqs. (39) and (40) and shown as color surfaces in Figure (7). The black dots represent the finite element approximation of M_y and the SGR of $M_{y,x}$, respectively.

$$M_y(x,y) = D\left(\frac{\partial^2 w}{\partial y^2} + \nu\frac{\partial^2 w}{\partial x^2}\right) = \frac{q_0}{\pi^2}\frac{\left(a^4b^2 + \nu a^2b^4\right)}{\left(a^2+b^2\right)^2}\sin\frac{\pi x}{a}\sin\frac{\pi y}{b} \tag{39}$$

$$M_{y,x}(x,y) = D\frac{\partial}{\partial x}\left(\frac{\partial^2 w}{\partial y^2} + \nu\frac{\partial^2 w}{\partial x^2}\right) = \frac{q_0}{\pi}\frac{\left(a^3b^2 + \nu ab^4\right)}{\left(a^2+b^2\right)^2}\cos\frac{\pi x}{a}\sin\frac{\pi y}{b} \tag{40}$$

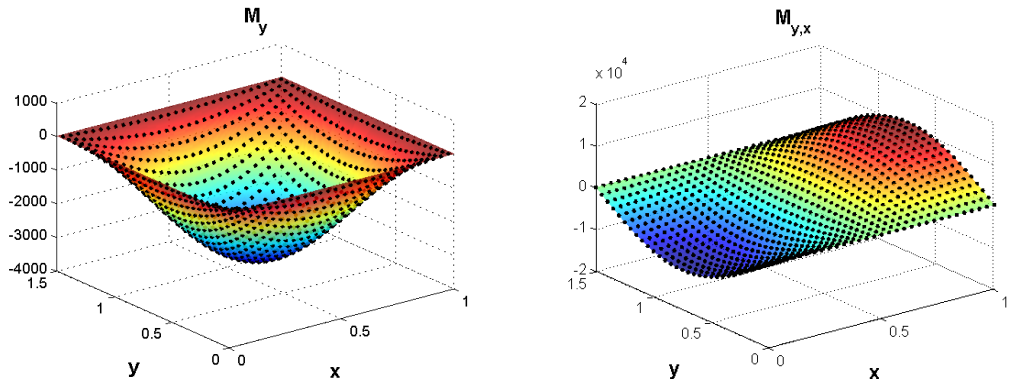

Figure 7. Moment about x-axis, M_y (left) and Spatial Derivative of Moment about x-axis, $M_{y,x}$ (right)

Here, the moment gradients, $M_{x,x}$ and $M_{y,x}$, are reconstructed directly from the finite element approximation of the moments, M_x and M_y on the left hand sides of Eqs. (37) and (39). Whereas following the implementation of Duvigneau and Pelletier[22] the moment gradients, $M_{x,x}$ and $M_{y,x}$, would be reconstructed from higher order derivatives of w. The latter requires specific knowledge of the boundary operator formulation, whereas applying SGR directly to secondary variables does not.

5. *Local Sensitivity Equations and Boundary Conditions*

The governing equation of the local sensitivity system is

$$A(w';\boldsymbol{b}) = \frac{\partial^4 w'}{\partial x^4} + 2\frac{\partial^2 w'}{\partial x^2}\frac{\partial^2 w'}{\partial y^2} + \frac{\partial^4 w'}{\partial y^4} = f'(x,y;\boldsymbol{b}) \tag{41}$$

Where, $f'(x,y;\boldsymbol{b})$ is the local sensitivity of the distributed load and is formulated in Eq. (42). Recall from Eq.(4) that $(\cdot)'$ denotes a partial derivative with respect to the design variable. In this case, the design variable is the plate dimension a.

$$f'(x,y;\boldsymbol{b}) = -\frac{q_0}{D}\frac{\pi}{a^2}x\cos\frac{\pi x}{a}\sin\frac{\pi y}{b} \tag{42}$$

Figure (8) shows the distributed load, $f'(x,y;\boldsymbol{b})$ which is applied to the local sensitivity system. Here the analytic expression is represented by the color surface, while the black dots represent the integrated sensitivity force values that are applied to the discretized local sensitivity system.

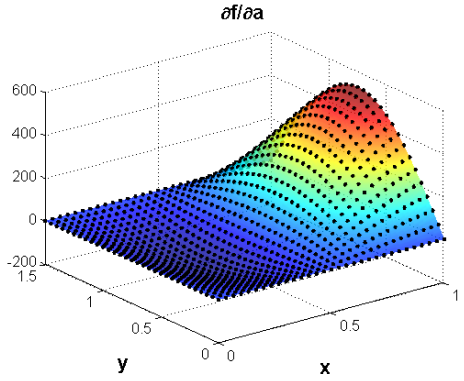

Figure 8. Local Sensitivity of Distributed Load w.r.t. a

The local sensitivity boundary conditions are derived using the standard definitions formulated in Eqs. (29) and (30). The local sensitivity boundary conditions at $x = 0$ are

$$w'(0,y) = \dot{w}(0,y) - w_{,x}(0,y)\mathcal{V}(0,y) = 0 - w_{,x}(0,y)\cdot 0 = 0 \tag{43}$$

$$\psi'_x(0,y) = \dot{\psi}_x(0,y) - \psi_{x,x}(0,y)\mathcal{V}(0,y) = 0 - \psi_{x,x}(0,y)\cdot 0 = 0 \tag{44}$$

$$M'_x(0,y) = \dot{M}_x(0,y) - M_{x,x}(0,y)\mathcal{V}(0,y) = 0 - M_{x,x}(0,y)\cdot 0 = 0 \tag{45}$$

The local sensitivity boundary conditions at $x = a$ are

$$w'(a,y) = \dot{w}(a,y) - w_{,x}(a,y)\mathcal{V}(a,y) = 0 - w_{,x}(a,y)\cdot 1 = \frac{q_0}{D\pi^3}\frac{a^3b^4}{\left(a^2+b^2\right)^2}\sin\frac{\pi y}{b} \tag{46}$$

$$\psi'_x(a,y) = \dot{\psi}_x(a,y) - \psi_{x,x}(a,y)\mathcal{V}(a,y) = 0 - \psi_{x,x}(a,y)\cdot 1 = \frac{q_0}{D\pi^2}\frac{a^3b^3}{\left(a^2+b^2\right)^2}\cos\frac{\pi y}{b} \tag{47}$$

$$M'_x(a,y) = \dot{M}_x(a,y) - M_{x,x}(a,y)\mathcal{V}(a,y) = 0 - M_{x,x}(a,y)\cdot 1 = \frac{q_0}{\pi}\frac{\left(ab^4+\nu a^3b^2\right)}{\left(a^2+b^2\right)^2}\sin\frac{\pi y}{b} \tag{48}$$

The local sensitivity boundary conditions at $y = 0$ are

$$w'(x,0) = \dot{w}(x,0) - w_{,x}(x,0)\mathcal{V}(x,0) = 0 - 0\cdot\frac{x}{a} = 0 \tag{49}$$

$$M'_y(x,0) = \dot{M}_y(x,0) - M_{y,x}(x,0)\mathcal{V}(x,0) = 0 - 0\cdot\frac{x}{a} = 0 \tag{50}$$

$$\psi'_y(x,0) = \dot{\psi}_y(x,0) - \psi_{y,x}(x,0)\mathcal{V}(x,0) = 0 - 0\cdot\frac{x}{a} = 0 \tag{51}$$

The local sensitivity boundary conditions at $y = b$ are

$$w'(x,b) = \dot{w}(x,b) - w_{,x}(x,b)\mathcal{V}(x,b) = 0 - 0\cdot\frac{x}{a} = 0 \tag{52}$$

$$M'_y(x,b) = \dot{M}_y(x,b) - M_{y,x}(x,b)\mathcal{V}(x,b) = 0 - 0\cdot\frac{x}{a} = 0 \tag{53}$$

$$\psi'_y(x,b) = \dot{\psi}_y(x,b) - \psi_{y,x}(x,b)\mathcal{V}(x,b) = 0 - 0\cdot\frac{x}{a} = 0 \tag{54}$$

Figure (9) shows the analytic local sensitivity boundary conditions as compared to those computed from the finite element solution using SGR. The SGR accurately approximates the local sensitivity boundary conditions at $x = 0$ and $x = a$ as shown in the upper plots of Figure (9). At $y = 0$ and $y = b$ the analytic local sensitivity boundary conditions are zero. The numerical error that the SGR introduces into the local sensitivity boundary conditions is obvious in the lower plots of Figure (9). Numerical error in the sensitivity boundary conditions results in numerical error in the sensitivity solutions. Refining the mesh and enhancing the SGR routine provide a means to reduce and potentially eliminate the numerical error.

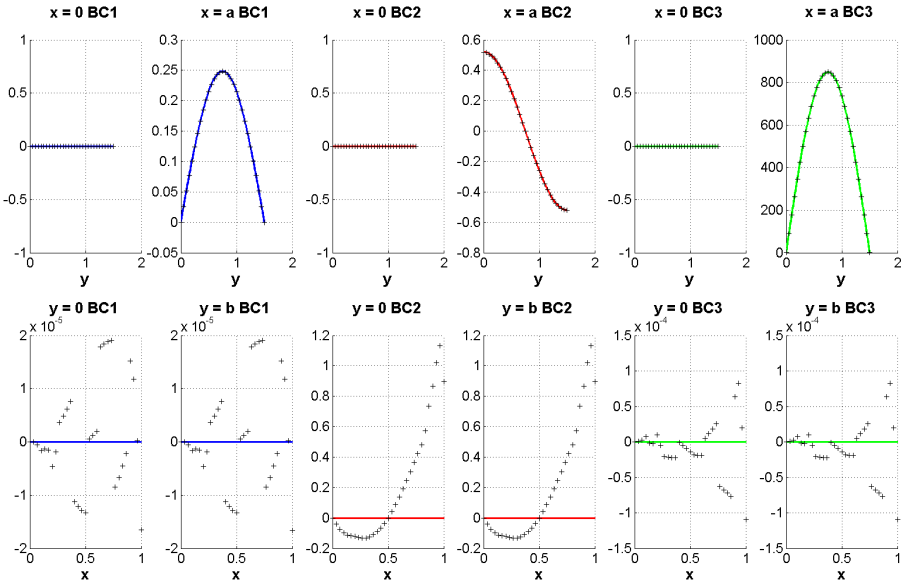

Figure 9. Local sensitivity boundary conditions corresponding to Eqs. (43-48) in the upper plots and Eqs. (49-54) in the lower plots

6. *Local Sensitivities*

Directly differentiating Eqs. (31-33) with respect to the plate length, a, yields the analytic local sensitivity solutions of transverse displacement, rotation about the x-axis, and rotation about the y-axis.

$$w'(x,y) = -\frac{q_0}{D\pi^3}\frac{a^2b^4}{\left(a^2+b^2\right)^2}x\cos\frac{\pi x}{a}\sin\frac{\pi y}{b} + \frac{q_0}{D\pi^4}\frac{4}{\left(a^2+b^2\right)^2}\left(-\frac{a^5b^4}{\left(a^2+b^2\right)}+a^3b^4\right)\sin\frac{\pi x}{a}\sin\frac{\pi y}{b} \tag{55}$$

$$\psi_x'(x,y) = -\frac{q_0}{D\pi^2}\frac{a^2b^3}{\left(a^2+b^2\right)^2}x\cos\frac{\pi x}{a}\cos\frac{\pi y}{b} + \frac{q_0}{D\pi^3}\frac{4}{\left(a^2+b^2\right)^2}\left(-\frac{a^5b^3}{\left(a^2+b^2\right)}+a^3b^3\right)\sin\frac{\pi x}{a}\cos\frac{\pi y}{b} \tag{56}$$

$$\psi_y'(x,y) = -\frac{q_0}{D\pi^2}\frac{ab^4}{\left(a^2+b^2\right)^2}x\sin\frac{\pi x}{a}\sin\frac{\pi y}{b} + \frac{q_0}{D\pi^3}\frac{1}{\left(a^2+b^2\right)^2}\left(\frac{4a^4b^4}{\left(a^2-b^2\right)}+3a^2b^4\right)\cos\frac{\pi x}{a}\sin\frac{\pi y}{b} \tag{57}$$

Figure (10) shows the local continuum sensitivity solution as compared to the analytic local sensitivity. The accuracy of the method is quantified in a later section. For now it appears that the numerical error in the local sensitivity boundary conditions has a minimal impact on the solution.

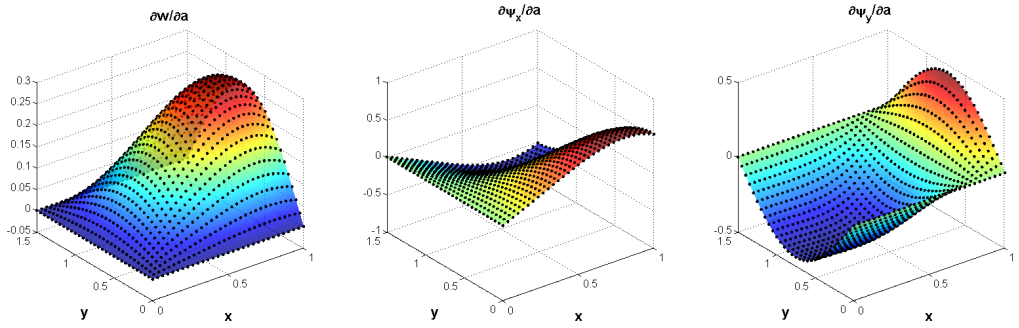

Figure 10. Local Sensitivity of Displacements w.r.t. a

7. *Total Sensitivities*

The analytic total sensitivity solutions of transverse displacement, rotation about the x-axis, and rotation about the y-axis are are found by taking the material derivative of Eqs. (31-33).

$$\dot{w}(x,y) = \frac{q_0}{D\pi^4}\frac{4}{\left(a^2+b^2\right)^2}\left(-\frac{a^5b^4}{\left(a^2+b^2\right)}+a^3b^4\right)\sin\frac{\pi x}{a}\sin\frac{\pi y}{b} \tag{58}$$

$$\dot{\psi}_x(x,y) = \frac{q_0}{D\pi^3}\frac{4}{\left(a^2+b^2\right)^2}\left(-\frac{a^5b^3}{\left(a^2+b^2\right)}+a^3b^3\right)\sin\frac{\pi x}{a}\cos\frac{\pi y}{b} \tag{59}$$

$$\dot{\psi}_y(x,y) = \frac{q_0}{D\pi^3}\frac{1}{\left(a^2+b^2\right)^2}\left(\frac{4a^4b^4}{\left(a^2+b^2\right)}-3a^2b^4\right)\cos\frac{\pi x}{a}\sin\frac{\pi y}{b} \tag{60}$$

Figure (11) shows the total sensitivity solution as compared to the analytic total sensitivity. The total sensitivity was computed by adding the convective term according to Eq. (3) to the local sensitivity found by solving Eq. (41) subject to Eqs. (43-54). Eqs. (55) through (60) satisfy the relationship between the local and total derivatives as formulated in Eq. (3).

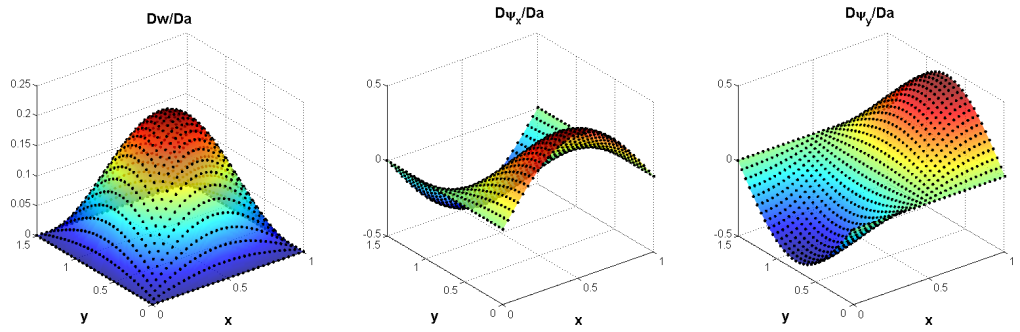

Figure 11. Total Sensitivity of Displacements w.r.t. a

The continuum sensitivity solution computed from the finite element analysis results using SGR appears in Figure (11) to be satisfactorily accurate. The accuracy of the method is quantified in the following mesh convergence study.

8. *Mesh Convergence Study*

There are, primarily, three potential sources of error in the local continuum sensitivity solution. They are: the discretization error from the original finite element analysis, the error from the SGR computation, and the discretization error from the sensitivity finite element analysis. The accuracy of transverse displacement, w, the spatial derivative in the x-direction of transverse displacement, $w_{,x}$, and the total sensitivity of transverse displacement, $\dot{w}$ are quantified for a range of mesh sizes. The study includes 8-noded serendipity quadrilateral elements (CQUAD8) in addition to the bilinear CQUAD4 elements. Furthermore, the accuracy when applying an uniform distributed load is investigated in addition to the sinusoidal distributed load examined in the last section. The analytic solution for the case of the uniform load can also be found in Timoshenko's *Theory of Plates and Shells*.[25] The errors are displayed graphically in Figure (12) and they are also presented numerically in Tables (1) and (2).

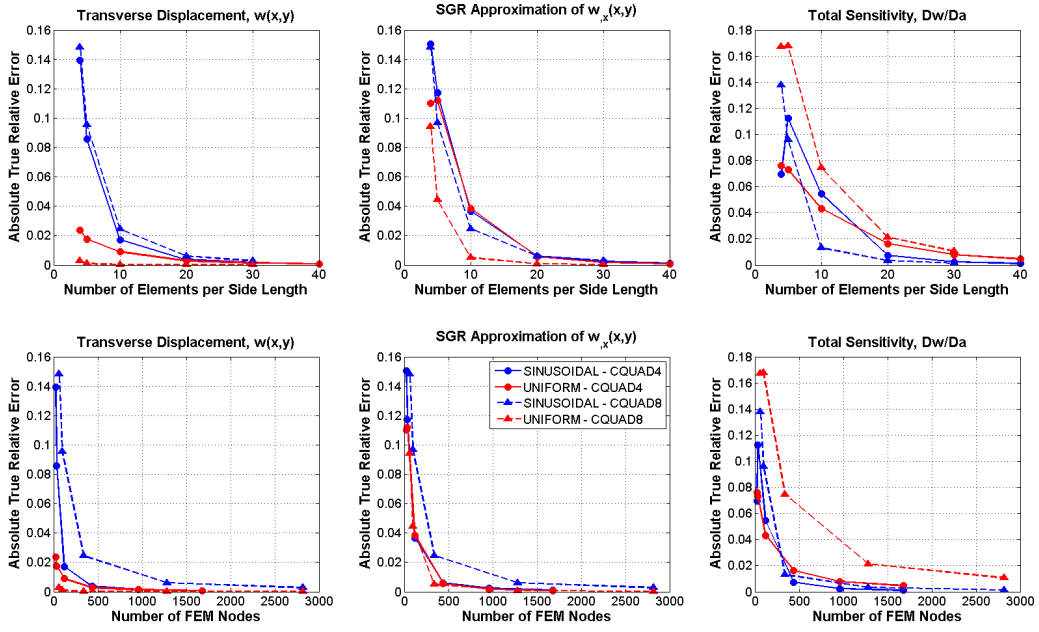

Figure 12. Mesh Convergence Results: Error vs. Number of elements per side (top row), Error vs. Number of Nodes (bottom row), Transverse Displacement (left column), SGR of x-derivative of Transverse Displacement (middle column), Local Continuum Result of Total Transverse Displacement Sensitivity (right column)

		Sinusoidal			Uniform		
No. Elem	No. Nodes	w	$w_{,x}$	$\dot{w}$	w	$w_{,x}$	$\dot{w}$
4	25	13.95	15.05	6.93	2.36	11.03	7.59
5	36	8.59	11.73	11.22	1.77	11.21	7.32
10	121	1.71	3.67	5.45	0.90	3.83	4.33
20	441	0.35	0.61	0.72	0.29	0.57	1.64
30	961	0.15	0.23	0.25	0.13	0.18	0.79
40	1681	0.08	0.10	0.12	0.08	0.08	0.46

Table 1. CQUAD4 Absolute True Percent Relative Errors for Mesh Convergence

		Sinusoidal			Uniform		
No. Elem	No. Nodes	w	$w_{,x}$	$\dot{w}$	w	$w_{,x}$	$\dot{w}$
4	65	14.83	14.82	13.78	0.30	9.42	16.75
5	96	9.56	9.70	9.60	0.10	4.45	16.77
10	341	2.45	2.47	1.30	0.009	0.50	7.45
20	1281	0.61	0.61	0.34	0.002	0.07	2.13
30	2821	0.27	0.28	0.14	0.001	0.02	1.06

Table 2. CQUAD8 Absolute True Percent Relative Errors for Mesh Convergence

The study demonstrates strong convergence for all of the cases. Convergence of the spatial derivative demonstrates that the SGR computation is adequate. Therefore, the same Taylor series and patch definitions were sued to carry out the remainder of the examples in this paper. The relative slower convergence of the sensitivity for CQUAD8 elements under a uniform load. This is most likely caused by the integration of the force intensities output by Nastran being inconsistent with the integration used by Nastran. This is something that will be considered in future work.

Also demonstrated by this study is the ease by which sensitivities are calculated for the different element types and different loading conditions. The sensitivity approach is independent of the element formulation and operates solely on analysis output. Therefore, the sensitivity algorithm does not need any adjustments when running the different cases shown in this convergence study. This would not be possible when implementing other analytic sensitivity methods.

C. Square Plate with a 2-D Design Velocity Field

The following example shows shape sensitivity results for a square plate that is parameterized by a single variable, s, the side length of the plate. This means that when the geometry is perturbed, all sides of the plate lengthen, which means that the design velocity is nonzero in both the x- and y- directions. The properties of the plate for the solution shown here are the same as in the previous example, except now $a = b = s = 1m$. All edges of the plate are simply-supported, and the plate is subjected to a sinusoidal distributed transverse load. The finite element analysis was conducted on a 30 by 30 mesh of CQUAD4 plate elements. The local continuum sensitivity solution for this model is compared to finite difference sensitivities.

The displacement solution is shown in Figure (13). Here the finite element solution is not being compared to an analytic solution. Therefore, the black dots are the results at the finite element nodes, and the surfaces are simply an interpolation of these.

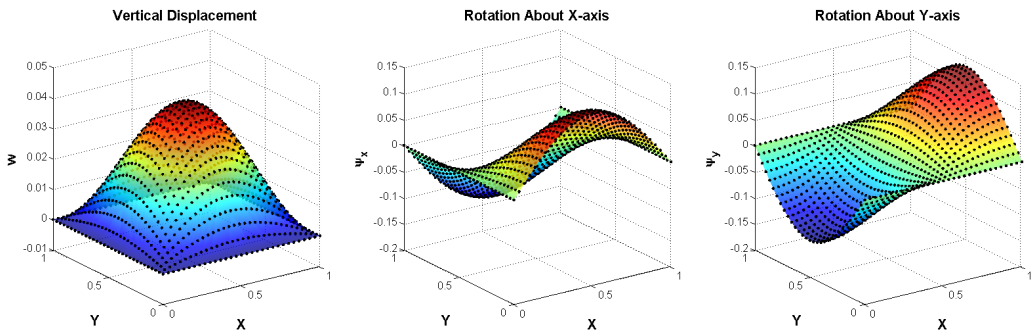

Figure 13. Displacements

The distributed load on the plate is

$$f(x,y;\boldsymbol{b}) = q_0 \sin\frac{\pi x}{s}\sin\frac{\pi y}{s} \tag{61}$$

Therefore, the distributed load on the sensitivity system, $f'(x,y;\boldsymbol{b})$ is

$$f'(x,y;\boldsymbol{b}) = -\frac{\pi q_0}{s^2}\left(x\cos\frac{\pi x}{s}\sin\frac{\pi y}{s} + y\sin\frac{\pi x}{s}\cos\frac{\pi y}{s}\right) \tag{62}$$

The design velocity field is defined as

$$\boldsymbol{\mathcal{V}} = \frac{x}{s}\hat{x} + \frac{y}{s}\hat{y} \tag{63}$$

The local sensitivity boundary conditions at $x = 0$ are

$$w'(0,y) = \dot{w}(0,y) - w_{,x}(0,y)\mathcal{V}_x(0,y) - w_{,y}(0,y)\mathcal{V}_y(0,y) = -w_{,y}(0,y)\cdot\frac{y}{s} \tag{64}$$

$$\psi_x'(0,y) = \dot{\psi}_x(0,y) - \psi_{x,x}(0,y)\mathcal{V}_x(0,y) - \psi_{x,y}(0,y)\mathcal{V}_y(0,y) = -\psi_{x,y}(0,y)\cdot\frac{y}{s} \tag{65}$$

$$M_x'(0,y) = \dot{M}_x(0,y) - M_{x,x}(0,y)\mathcal{V}_x(0,y) - M_{x,y}(0,y)\mathcal{V}_y(0,y) = -M_{x,y}(0,y)\cdot\frac{y}{s} \tag{66}$$

The local sensitivity boundary conditions at $x = s$ are

$$w'(s,y) = \dot{w}(s,y) - w_{,x}(s,y)\mathcal{V}_x(s,y) - w_{,y}(s,y)\mathcal{V}_y(s,y) = -w_{,x}(s,y) - w_{,y}(s,y)\cdot\frac{y}{s} \tag{67}$$

$$\psi_x'(s,y) = \dot{\psi}_x(s,y) - \psi_{x,x}(s,y)\mathcal{V}_x(s,y) - \psi_{x,y}(s,y)\mathcal{V}_y(s,y) = -\psi_{x,x}(s,y) - \psi_{x,y}(s,y)\cdot\frac{y}{s} \tag{68}$$

$$M_x'(s,y) = \dot{M}_x(s,y) - M_{x,x}(s,y)\mathcal{V}_x(s,y) - M_{x,y}(s,y)\mathcal{V}_y(s,y) = -M_{x,x}(s,y) - M_{x,y}(s,y)\cdot\frac{y}{s} \tag{69}$$

The local sensitivity boundary conditions at $y = 0$ are

$$w'(x,0) = \dot{w}(x,0) - w_{,x}(x,0)\mathcal{V}_x(x,0) - w_{,y}(x,0)\mathcal{V}_y(x,0) = -w_{,x}(x,0)\cdot\frac{x}{s} \tag{70}$$

$$M_y'(x,0) = \dot{M}_y(x,0) - M_{y,x}(x,0)\mathcal{V}_x(x,0) - M_{y,y}(x,0)\mathcal{V}_y(x,0) = -M_{y,x}(x,0)\cdot\frac{x}{s} \tag{71}$$

$$\psi_y'(x,0) = \dot{\psi}_y(x,0) - \psi_{y,x}(x,0)\mathcal{V}_x(x,0) - \psi_{y,y}(x,0)\mathcal{V}_y(x,0) = -\psi_{y,x}(x,0)\cdot\frac{x}{s} \tag{72}$$

The local sensitivity boundary conditions at $y = s$ are

$$w'(x,s) = \dot{w}(x,s) - w_{,x}(x,s)\mathcal{V}_x(x,s) - w_{,y}(x,s)\mathcal{V}_y(x,s) = -w_{,x}(x,s)\cdot\frac{x}{s} - w_{,y}(x,s) \tag{73}$$

$$M_y'(x,s) = \dot{M}_y(x,s) - M_{y,x}(x,s)\mathcal{V}_x(x,s) - M_{y,y}(x,s)\mathcal{V}_y(x,s) = -M_{y,x}(x,s)\cdot\frac{x}{s} - M_{y,y}(x,s) \tag{74}$$

$$\psi'_y(x,s) = \dot{\psi}_y(x,s) - \psi_{y,x}(x,s)\mathcal{V}_x(x,s) - \psi_{y,y}(x,s)\mathcal{V}_y(x,s) = -\psi_{y,x}(x,s)\cdot\frac{x}{s} - \psi_{y,y}(x,s) \tag{75}$$

Since the design velocity is non-zero in both the x- and y-directions, the local sensitivity boundary conditions are now dependent on spatial derivatives in both the x- and y-directions. The local sensitivity solution is shown in Figure (14). The total sensitivity solution is shown in Figure (15). In these two figures the surface is an interpolation of the local continuum sensitivity solution at the finite element nodes, and the blue dots are the finite difference sensitivity solution at the finite element nodes. A relative step size of $1e-4$ was used to compute the finite difference sensitivities.

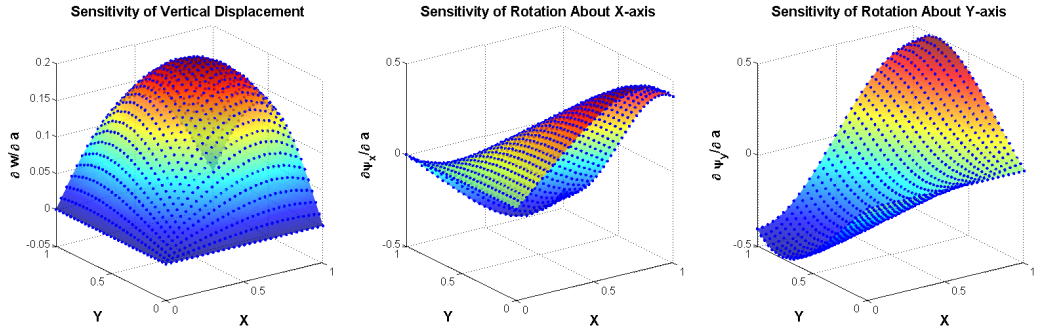

Figure 14. Local Sensitivity of Displacements w.r.t. s

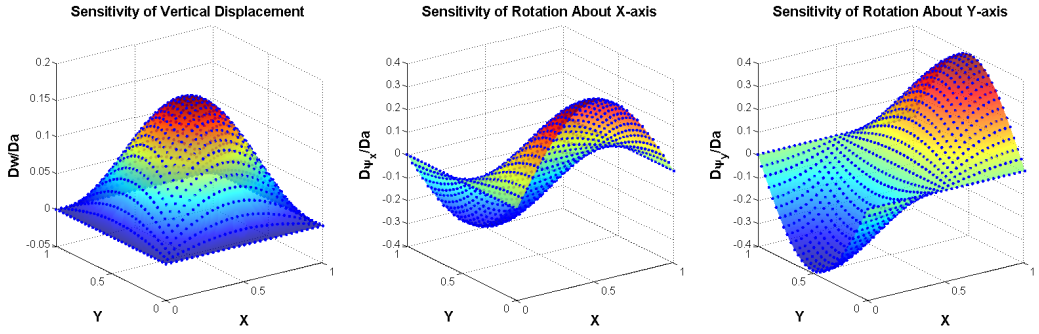

Figure 15. Total Sensitivity of Displacements w.r.t. s

The results indicate strong agreement between the local continuum and finite difference sensitivity methods. Furthermore, it demonstrates that the local continuum method is successful for a 2-D design velocity field. Another noteworthy observation is that the total sensitivity fields are very similar in shape to the total sensitivity fields of the previous example, but the local sensitivity fields are drastically different.

D. Kirchhoff vs. Reissner-Midlin Plate Theory

One major advantage of the local continuum sensitivity method being presented here is, it truly can be implemented with a black box analysis. To demonstrate this, the finite element results of modeling a thick rectangular plate under a uniform distributed transverse load with Kirchhoff plate theory is compared to the finite element results of modeling the same plate with Reissner-Midlin plate theory. In Nastran, this is done by simply turning on and off the transverse shear flexibility of the plate elements.

The properties of the plate for the solutions shown here are $a = b = 1m$, $q_0 = 10e6N/m$, $E = 7e9N/m^2$, $t = 0.1m$, and $\nu = 0.75$. To also demonstrate the capability of handling mixed boundary conditions, the $x = 0$ and $y = 0$ edges of the plate are clamped, while the $x = a$ and $y = b$ edges of the plate are simply-supported. The finite element analysis is conducted on a 40 by 40 mesh of CQUAD4 elements. The local continuum sensitivity results are compared to finite difference sensitivities.

The displacement solutions for the Kirchhoff and Reissner-Midlin plates are shown in Figures (16) and (17). The transverse displacement is significantly larger for the Reissner-Midlin plate, which is expected because the shear effects are significantly greater for thick plates.

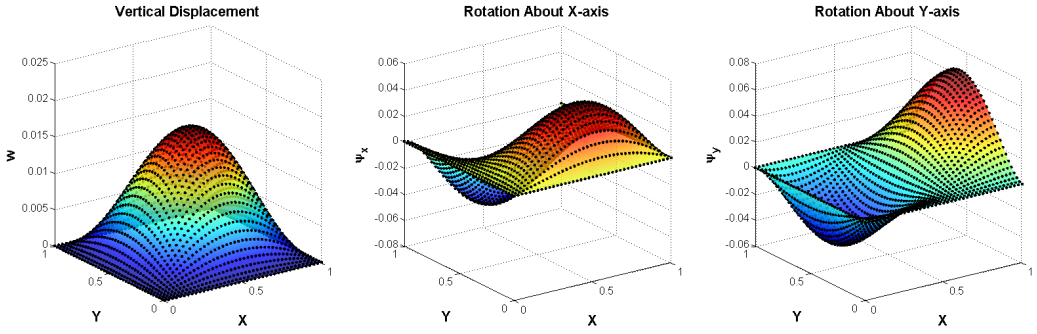

Figure 16. Kirchhoff Plate Displacements

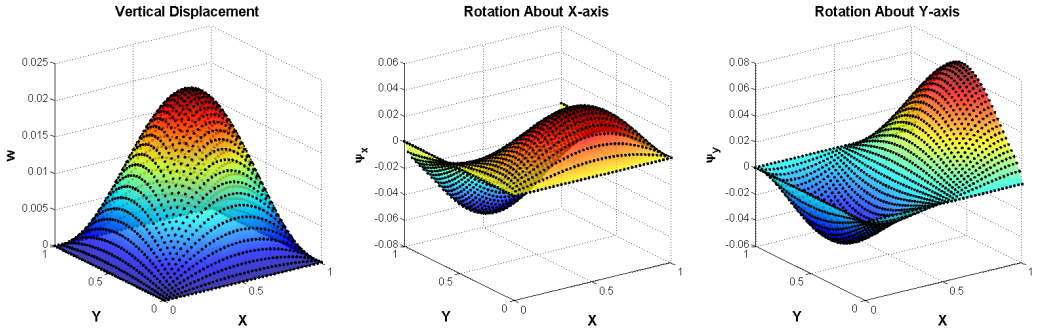

Figure 17. Reissner-Midlin Plate Displacements

The local sensitivity solutions for the Kirchhoff and Reissner-Midlin plates are shown in Figures (18) and (19), respectively. The sensitivity is with respect to the plate dimension a. The key advantage demonstrated here is that the local continuum sensitivities are calculated using the exact same algorithm. The algorithm is initiated by providing the following inputs: the geometry, the applied load, and the finite element analysis results. The latter, includes the linear stiffness matrix as output by Nastran, the displacement data, and the internal force data.

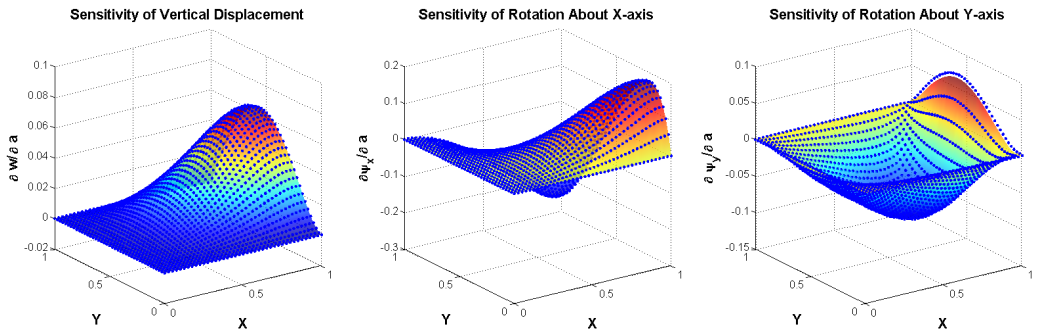

Figure 18. Kirchhoff Plate, Local Sensitivity of Displacements w.r.t. a

The algorithm does not require information regarding the type of plate theory used, or more generally, it does not require any information regarding the element formulation (theory, shape functions, etc.).

Implementing discrete and total continuum analytic sensitivity methods for these two different models requires individual derivations, one for each plate theory. Furthermore, both the discrete and total continuum methods require the derivative of the stiffness matrix, which requires individual sensitivity derivations for different types of shape functions. The local continuum sensitivity method presented here eliminates these dependencies, and generalizes the sensitivity algorithm in a dramatic way.

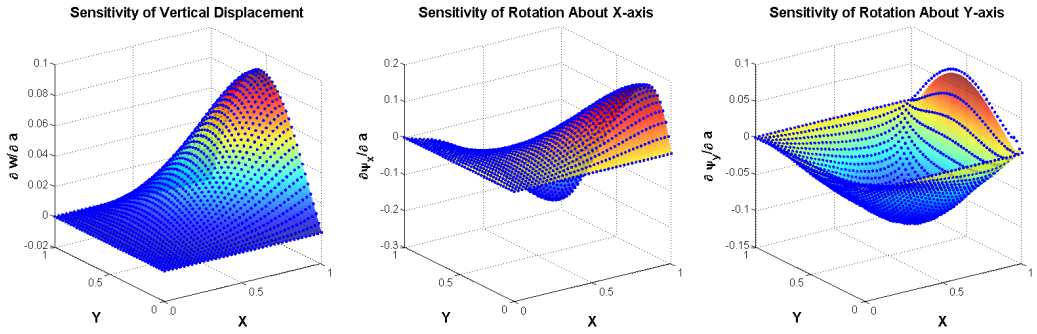

Figure 19. Reissner-Midlin Plate, Local Sensitivity of Displacements w.r.t. a

V. Continuum Sensitivity Implementation for Beam-Stiffened Plate Models

A. Beam-Stiffened Plate Model I

The local continuum sensitivity method requires additional boundary conditions to be implemented at structural interfaces where stress and/or strain discontinuities are present. This is one reason that the discrete analytic and total continuum sensitivity methods are more commonly used. Accounting for said discontinuities is not required by them. The following example is a comparison of a local continuum sensitivity solution and a finite difference sensitivity solution of a beam-stiffened rectangular plate under a uniform distributed transverse loading. This example demonstrates how to account for systems that have stress and/or strain discontinuities at structural interfaces.

1. Model Information

The same rectangular plate model in the previous analytic example is used again here. The properties of the plate are unchanged. The plate, however, is modified by a stiffener that is placed along the $x = a/2 = 0.5m$ axis. The stiffener is modeled as a beam having $E = 7e10N/m^2$, $G = 26e9N/m^2$, $A = 0.0025m^2$, and $I = 1e-6m^4$. The structural nodes of the beam are coincident with the structural nodes of the plate that lie on the $x = 0.5m$ axis. The neutral axis of the beam is not offset from the nodes, but it is expected that an offset does not affect the sensitivity formulation. However, offsets will be included in future implementations. All edges of the plate are simply-supported, and the finite element analysis is conducted on a 60 by 60 mesh of CQUAD4 elements.

2. Displacements of Beam-Stiffened Model

The displacement solution of the stiffened plate is shown in Figure (20). The unstiffened plate has a maximum deflection equal to approximately $7cm$, and adding the stiffener reduces the maximum deflection to approximately $2cm$. Spatial gradient reconstruction yields the displacement gradient fields shown in Figure (21).

The beam introduces a discontinuity in the through-thickness shear strain, which corresponds to the second order derivatives of ψ_x and ψ_y. The sensitivity boundary conditions only depend on the spatial derivatives shown in Figure (21), and do not include second order derivatives. Therefore, the shear strain discontinuity does not affect the local sensitivity boundary conditions. However, the following subsection shows that force discontinuities do play a role in the local sensitivity boundary conditions.

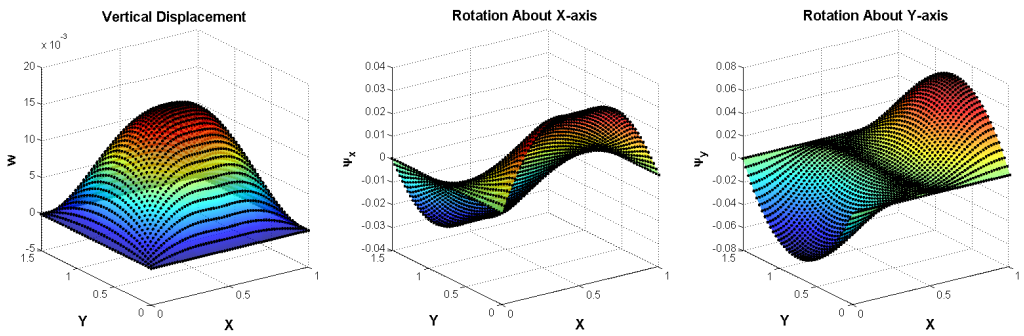

Figure 20. Displacements of the Beam-Stiffened Plate

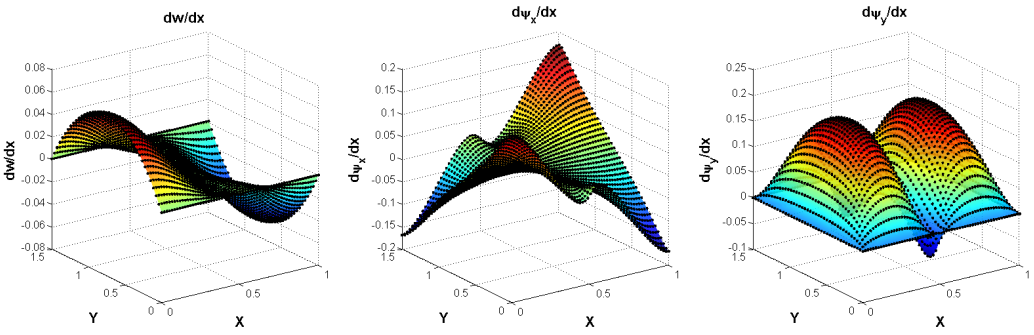

Figure 21. Displacement Gradients of the Beam-Stiffened Plate

3. Internal Forces of Beam-Stiffened Model

Applying SGR to the finite element force solution of the stiffened plate yields the force gradients shown in Figure (22). The discontinuities in the moment gradients require that a force boundary condition be applied to the sensitivity system at the structural interface, as described next.

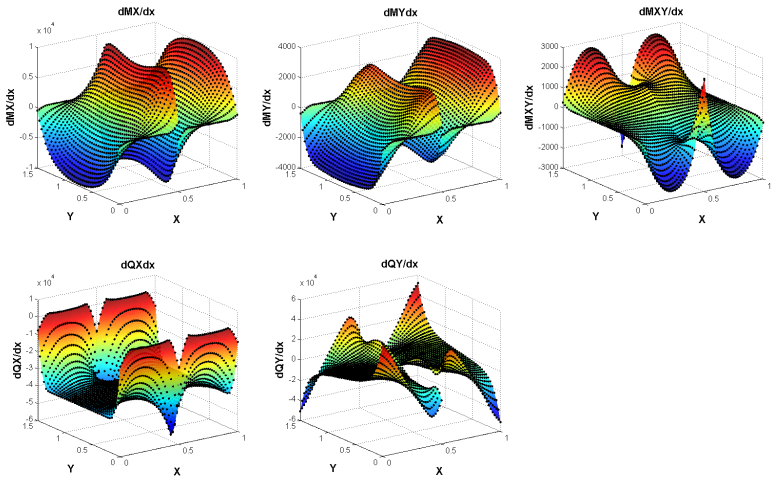

Figure 22. Force Gradients of the Beam-Stiffened Plate

4. Structural Interface Boundary Condition and Sensitivity Results

The local continuum sensitivity system is formulated with the same boundary conditions as the non-stiffened plate, only now the beam does apply a stiffening force along the $x = 0.5m$ axis of the plate. Following the boundary condition formulation for discontinuous sensitivity variables in Ref. (19), the additional local sensitivity boundary conditions are

$$V'_y(\frac{a^+}{2}, y) = \left(V_{y,x}(\frac{a^+}{2}, y) - V_{y,x}(\frac{a^-}{2}, y)\right) \mathcal{V}(\frac{a}{2}, y) \tag{76}$$

$$M'_x(\frac{a^+}{2}, y) = \left(M_{x,x}(\frac{a^+}{2}, y) - M_{x,x}(\frac{a^-}{2}, y)\right) \mathcal{V}(\frac{a}{2}, y) \tag{77}$$

$$M'_y(\frac{a^+}{2}, y) = \left(M_{y,x}(\frac{a^+}{2}, y) - M_{y,x}(\frac{a^-}{2}, y)\right) \mathcal{V}(\frac{a}{2}, y) \tag{78}$$

After solving the local continuum system, the resulting local sensitivities are converted to total sensitivities using the convective term. Both the local and total continuum sensitivity solutions are plotted along with the finite difference sensitivities (relative step size 1e-4) in Figures (23) and (24). The blue dots represent the finite difference sensitivity solution, while the surface is an interpolation of the continuum sensitivity solution.

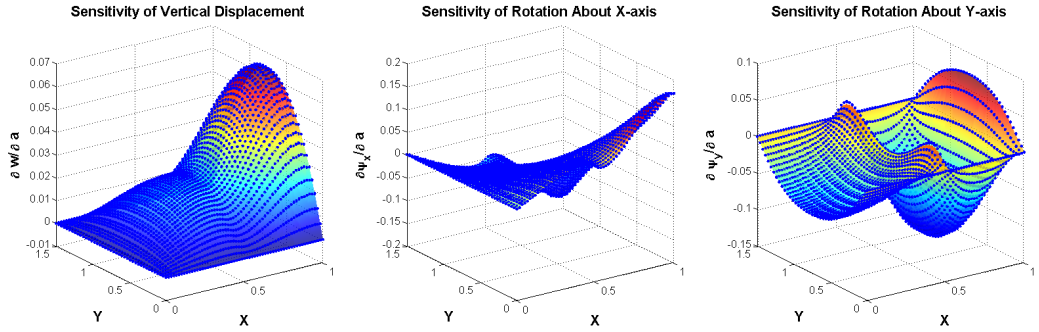

Figure 23. Local shape sensitivity w.r.t. a compared to finite difference sensitivity (blue dots)

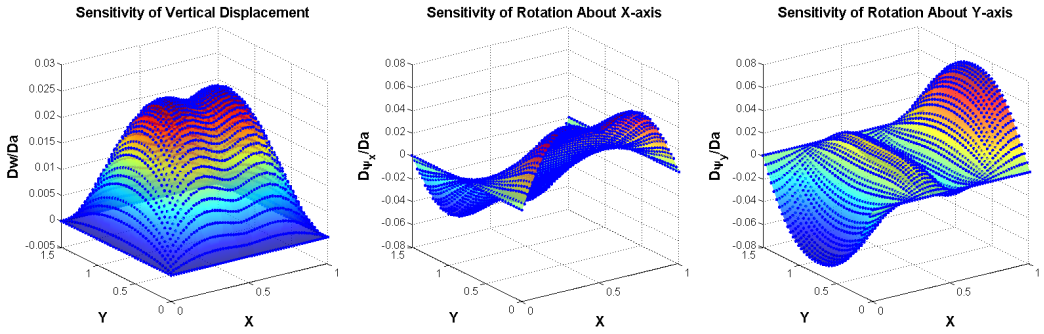

Figure 24. Total shape sensitivity w.r.t. a compared to finite difference sensitivity (blue dots)

The local continuum sensitivity method, as evidenced here, can yield accurate sensitivities for built-up structures. It is easy to imagine, however, a built-up structure with many structural interfaces requiring this type of boundary condition to be implemented. Therefore, one proposed approach to generalizing this method for built-up structures is to assemble the interface boundary condition at every structural interface. If a discontinuity is present, than it is captured appropriately, and if a discontinuity is not present, than the terms in Eqs. (76-78) which approach the interface from the + and - side will cancel and no additional force will be applied. The latter instance does increase the opportunity for introducing more numerical error into the local sensitivity boundary conditions, but it eliminates the need to know where the discontinuities are exactly.

VI. Conclusions

The discrete analytic and total continuum sensitivity methods require a rigorous formulation, derivation, and implementation. The structural fictitious load makes implementation with black box analyses infeasible. A local continuum sensitivity method was presented that eliminates the structural fictitious load from the sensitivity equations. Using a spatial gradient reconstruction technique, the local continuum sensitivity system can be formulated entirely from analysis output. The method is completely independent of the analysis formulation. This was demonstrated through the use of multiple element types and multiple plate theories while the sensitivity algorithm remained unchanged. Furthermore, mesh refinement showed that the sensitivity solutions converged to analytic solutions under multiple load conditions. Implementation of the sensitivity method for the beam-stiffened plate demonstrated that the approach is capable of handling built-up structures. In conclusion, the local continuum sensitivity method with spatial gradient reconstruction is a general approach to computing analytic sensitivities accurately. It is more readily able to be implemented for black box analyses and analyses of varying fidelity, than other analytic sensitivity methods.

Acknowledgments

This material is based on research sponsored by Air Force Research Laboratory under agreement number FA8650-09-2-3938. The U.S. Government is authorized to reproduce and distribute reprints for Governmental purposes notwithstanding any copyright notation thereon. The authors gratefully acknowledge the support of AFRL Senior Aerospace Engineers Dr. Raymond Kolonay, Dr. Ned Lindsley, and Dr. Jose Camberos.

References

[1]Cross, D. and Canfield, R.A. Continuum shape sensitivity with spatial gradient reconstruction of nonlinear aeroelastic gust response. *14th AIAA/ISSMO Multidisciplinary Analysis and Optimization Conference, Indianapolis, Indiana.*, AIAA 2012-5597.

[2]Liu, S., Wickert, P.D., and Canfield, R.A. Fluid-structure transient gust response sensitivity for a nonlinear joined wing model. *51st AIAA/ASME/ASCE/AHS/ASC Structures, Structural Dynamics, and Materials Conference, Orlando, Florida.*, AIAA 2010-3118, April 12-15, 2010.

[3]Arora, J. and Haug, E. Methods of design sensitivity analysis in structural optimization. *AIAA Journal*, Vol. 17, No. 9, Article No. 79-4109, 1979.

[4]Dems, K. and Haftka, R. Two approaches to sensitivity analysis for shape variation of structures. *Mech. Struct. and Mach.*, Vol. 16, No. 4, 1988-1989.

[5]Dems, K. and Mroz, Z. Variational approach to first- and second-order sensitivity analysis of elastic structures. *International Journal for Numerical Methods in Engineering*, Vol. 21, 1985.

[6]Bhaskaran, R. and Berkooz, G. Optimization of fluid-structure interaction using the sensitivity equation approach. *Fluid-Structure Interaction, Aeroelasticity, Flow-Induced Vibrations and Noise*, Vol. 1, No. 53-1, 1997.

[7]Choi, K. and Kim, N.H. *Structural Sensitivity Analysis and Optimization.* Springer Science + Business Media, 2005.

[8]Borggaard, J. and Burns, J. A sensitivity equation approach to shape optimization in fluid flows. *Technical Report, Langley Research Center*, 1994.

[9]Borggaard, J. and Burns, J. A pde sensitivity equation method for optimal aerodynamic design. *Journal of Computational Physics*, Vol. 136.

[10]Stanley, L. and Stewart, D. *Design sensitivity analysis: computational issues of sensitivity equation methods.* Academic Press, 2002.

[11]Turgeon, E., Pelletier, D., and Borggaard, J. A continuous sensitivity equation approach to optimal design in mixed convection. AIAA 99-3625.

[12]Etienne, S. and Pelletier, D. General approach to sensitivity analysis of fluid-structure interactions. *Journal of Fluids and Structures*, Vol. 21, No. 2.

[13]Wickert, D.P. and Canfield, R.A. Least-squares continuous sensitivity analysis of an example fluid-structure interaction problem. *49th AIAA/ASME/ASCE/AHS/ASC Structures, Structural Dynamics, and Materials Conference, Schaumberg, Illinois*, AIAA 2008-1896.

[14]Wickert, D.P., Canfield, R.A., and Reddy, J.N. Continuous sensitivity analysis of fluid-structure interaction problems using least-squares finite elements. *12th AIAA/ISSMO Multidisciplinary Analysis and Optimization Conference, Victoria, British Columbia, Canada.*, AIAA 2008-5931.

[15]Wickert, D.P., Canfield, R.A., and Reddy, J.N. Fluid-structure transient gust sensitivity using least-squares continuous sensitivity analysis. *50th AIAA/ASME/ASCE/AHS/ASC Structures, Structural Dynamics, and Materials Conference, Palm Springs, California.*, AIAA 2009-2535.

[16]Wickert, D.P. Least-squares, continuous sensitivity analysis for nonlinear fluid-structure interaction. *Dissertation, Air Force Institute of Technology.*, August 20, 2009.

[17]Liu, S. and Canfield, R.A. Continuum shape sensitivity for nonlinear transient aeroelastic gust response. *52nd AIAA/ASME/ASCE/AHS/ASC Structures, Structural Dynamics, and Materials Conference, Denver, Colorado.*, AIAA 2011-1971.

[18]Liu, S. and Canfield, R.A. Continuum shape sensitivity method for fluid flow around an airfoil. *53rd AIAA/ASME/ASCE/AHS/ASC Structures, Structural Dynamics, and Materials Conference, Honolulu, Hawaii.*, AIAA 2012-1426.

[19]Cross, D. and Canfield, R.A. Solving continuum shape sensitivity with existing tools for nonlinear aeroelastic gust analysis. *53rd AIAA/ASME/ASCE/AHS/ASC Structures, Structural Dynamics, and Materials Conference, Honolulu, Hawaii.*, AIAA 2012-1923.

[20]Haftka, R.T. and Adelman, H.M. Recent developments in structural sensitivity analysis. *Structural Optimization I*, 1989.

[21]Haftka, R. and Gurdal, Z. *Elements of Structural Optimization.* Kluwer Academic Publishers, 1992.

[22]Duvigneau, R. and Pelletier, D. On accurate boundary conditions for a shape sensitivity equation method. *International Journal for Numerical Methods in Fluids.*, Vol. 50.

[23]Akbari, J., Kim, N., and Ahmadi, M.T. Shape sensitivity analysis with design-dependent loadingsequivalence between continuum and discrete derivatives. *Structural and Multidisciplinary Optimization*, 2010.

[24]Zienkiewicz, O.C. and Zhu, J.Z. The superconvergent patch recovery and a posteriori error estimates. part 1: The recovery technique. *International Journal of Numerical Methods in Engineering*, Vol. 33.

[25]Timoshenko. *Theory of Plates and Shells.*

[26]Ricciardi, A.P., Patil, M.J., Canfield, R.A., and Lindsley, N. Utility of quasi-static gust loads certification methods for novel configurations. *52nd AIAA/ASME/ASCE/AHS/ASC Structures, Structural Dynamics, and Materials Conference, Denver, Colorado.*, AIAA 2011-2043, April 4-7, 2011.

[27]MSC Software Corporation. Md nastran 2010: User defined services. *MD Nastran Documentation.*

[28]MSC Software Corporation. Md nastran 2010: Dmap programmer's guide. *MD Nastran Documentation.*